Science of the Total Environment 726 (2020) 138535

Contents lists available at ScienceDirect

Science of the Total Environment

journal homepage: www.elsevier.com/locate/scitotenv

Renewable P-type zeolite for superior absorption of heavy metals: Isotherms, kinetics, and mechanism

Mingyue Chen [a], Shuying Nong [a], Yantao Zhao [a], Muhammad Sohail Riaz [a], Yi Xiao [a], Maxim S. Molokeev [b], Fuqiang Huang [a,c,*]

[a] Beijing National Laboratory for Molecular Sciences and State Key Laboratory of Rare Earth Materials Chemistry and Applications, College of Chemistry and Molecular Engineering, Peking University, Beijing 100871, China
[b] Siberian Federal University, Krasnoyarsk 660041, Russia
[c] CAS Key Laboratory of Materials for Energy Conversion and State Key Laboratory of High-Performance Ceramics and Superfine Microstructure, Shanghai Institute of Ceramics, Chinese Academy of Sciences, Shanghai 200050, China

HIGHLIGHTS

- The synthetic NASO zeolite without modification for eradicating heavy metals
- The great absorption capacities for Pb and Cd are 649 and 210 mg/g.
- Rapid purification for Pb wastewater to drinkable level is in 2 min.
- Adsorption involves both ion exchange reaction and electrostatic interaction.
- Concluding the determining factor affecting absorption capacity of zeolites

GRAPHICAL ABSTRACT

Herein, we firstly synthesized the octahedral zeolite $Na_6Al_6Si_{10}O_{32}\cdot 12H_2O$ without modification for eradicating heavy metal ions, proven great absorption capacity. Rapid adsorption and stable recycling performance made the zeolite to be promising for practical water purification and industrialization.

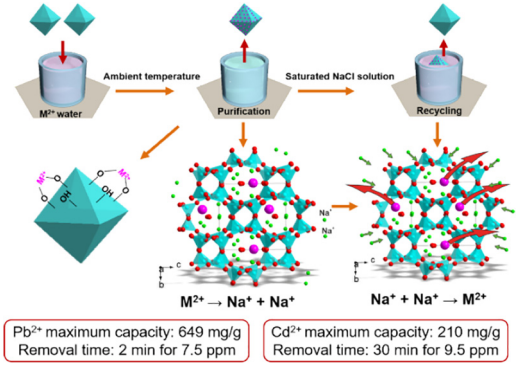

ARTICLE INFO

Article history:
Received 3 February 2020
Received in revised form 1 April 2020
Accepted 5 April 2020
Available online 8 April 2020

Editor: Deyi Hou

Keywords:
Uptake capacity

ABSTRACT

Zeolite is a characteristic material for removing heavy metals exhibiting by low tolerance quantities. It is particularly desirable although challenging to cultivate an unmodified and reusable zeolite for eradicating heavy metals with great capacity. Herein, we sought out and firstly synthesized the uniform octahedral zeolite $Na_6Al_6Si_{10}O_{32}\cdot 12H_2O$ for heavy metal ions trap, proven extraordinarily effective decontamination of M^{2+} (Pb^{2+}, Cd^{2+}, Cu^{2+}, and Zn^{2+}). The maximum capacities of Pb^{2+}, Cd^{2+}, Cu^{2+}, and Zn^{2+} were 649, 210, 90 and 88 mg/g, and the distribution coefficients (K_d) was ~10^8 mL/g for Pb^{2+} which emphasized the superior effectiveness of $Na_6Al_6Si_{10}O_{32}\cdot 12H_2O$ contrasted with other zeolites. Rapid adsorption was observed that Pb^{2+} concentration (7.5 ppm) was reduced to 0.6 ppb in 2 min. The removal mechanism was ascribed to the ion exchange and hydroxyl groups thereby affording high adsorption capacity. We also investigated the heavy metal removal

* Corresponding author at: Beijing National Laboratory for Molecular Sciences and State Key Laboratory of Rare Earth Materials Chemistry and Applications, College of Chemistry and Molecular Engineering, Peking University, Beijing 100871, China.
E-mail address: huangfq@pku.edu.cn (F. Huang).

https://doi.org/10.1016/j.scitotenv.2020.138535

High efficiency
Drinkable level
Regeneration

of zeolite 13X and 4A for comparison and concluded the determining factor affecting absorption capacity. The removal rate of Pb remained at 97% even after five regeneration recycles. The zeolite was therefore promising for practical water purification and industrialization.

1. Introduction

Heavy metal contamination, derived from batteries, electronics, electroplating, tanneries and petrochemicals, is becoming a core issue in environmental remediation due to toxicity and non-biodegradable, threatening human health via the entire food chain (Bolisetty and Mezzenga, 2016; Zhao et al., 2011). The adsorption in terms of high removal efficiency, renewable, environmentally friendly and flexibility in design and operation is considered to be a sustainable and economical technology for heavy metal removal. Until now, various adsorbents have been established for investigating removal performance and the adsorption mechanism of which mainly depend on ion exchange, complexation, and electrostatic attraction. Contemplating that complexation and electrostatic attraction are dominated by a surface-based process, many efforts should be devoted to the synthesis of absorbents with preferred structure and functionalized complex groups (Jawed et al., 2020; Li et al., 2014; Mukhopadhyay et al., 2020; Wu et al., 2019; Yang et al., 2019). The layered double hydroxides (LDHs) functionalized with polysulfide $[S_x]^{2-}$ and MoS_4^{2-} anions improve metal uptake capacity owing to the interaction between heavy metal cations and sulfide anions (Ma et al., 2016; Wang et al., 2019b). These absorbents are hard to prepare and inadequate for industrialization. Conversely, ion exchange is the reversible exchange of ions between the liquid phase and solid phase without any radical change of solid structure, which is widely utilized industrial technique in wastewater treatment as well as separation process due to reasonable cost and process simplicity. Diverse ion-exchange adsorbents, such as layered sulfides, zeolite (Qiu and Zheng, 2009), resin (Gossuin et al., 2020), clay (Sdiri et al., 2011; Uddin, 2017), are established for water treatment. The layered sulfides $K_xBi_{4-x}Mn_xS_6$, $K_{2x}Mn_xSn_{3-x}S_6$, $K_{2x}Sn_{4-x}S_{8-x}$ and $K_{0.48}Mn_{0.76}PS_3 \cdot H_2O$ demonstrate excellent removal efficacy of heavy metals through ion-exchange (Manos and Kanatzidis, 2009; Rathore et al., 2017; Sarma et al., 2016; Wang et al., 2019a). The exchange capacity of $K_xBi_{4-x}Mn_xS_6$ for Cd^{2+} and Pb^{2+} are 221 and 342 mg/g respectively and the K_d is ~10^7 mL/g. Unfortunately, the constancy and cycle property of sulfides is not impressive. Clay is a low-cost adsorbent, but they suffer from a weak affinity for heavy metals. Even though the ion exchange resin is a common absorbent for practical application, it will lead to secondary pollution.

Among ion-exchange absorbents, zeolites are microporous crystalline aluminosilicates that are well known for its uniform channels and cavities, which is especially suitable for water treatment contributed

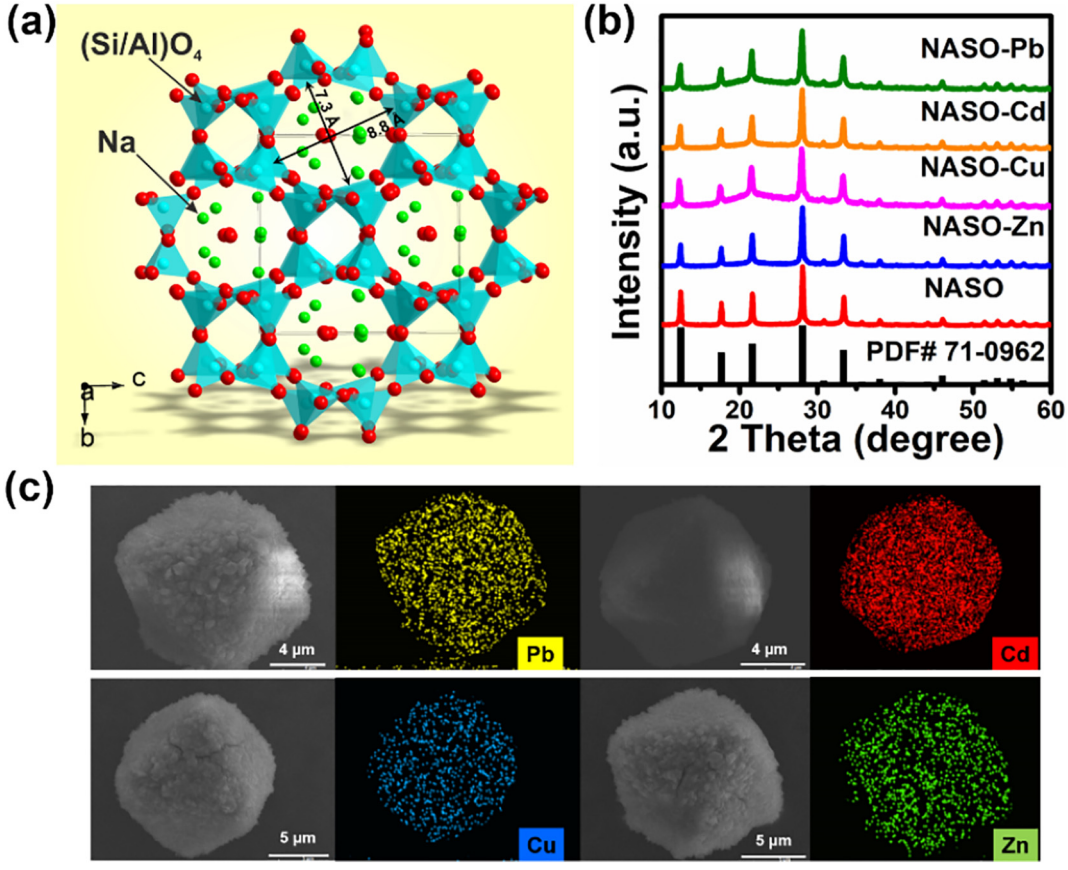

Fig. 1. (a) The crystal structure of NASO; (b) XRD patterns of NASO before and after adsorption of 10 ppm M^{2+}; (c) SEM images and EDS mapping for NASO after adsorption of M^{2+} with 10 ppm concentration.

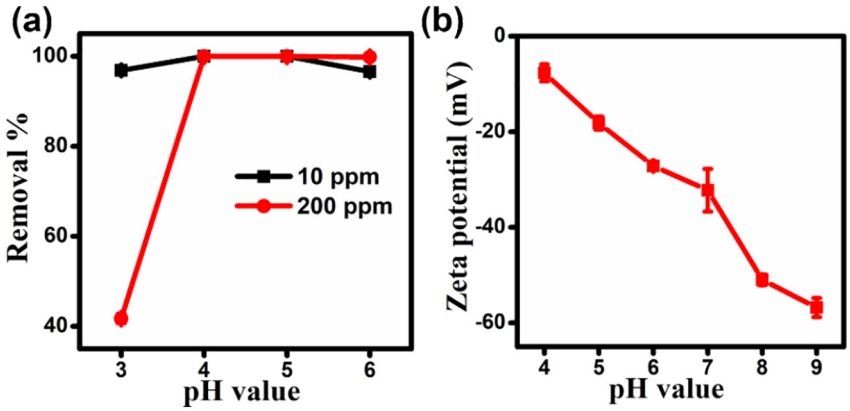

Fig. 2. (a) Effect of initial pH values on removal rates of different Pb^{2+} concentrations (10 and 200 ppm) by NASO; (b) zeta potential measurement plots of NASO at different pH values.

to easily attained, recycling and less secondary pollution (Tabit et al., 2019). Notably, they are low cost and accessible in bulk. The adsorption capacities of natural zeolites for Pb^{2+}, As^{5+}, Cu^{2+}, Zn^{2+} and Ni^{2+} are 125.2, 20.31, 14.65, 13.54 and 11.68 mg/g respectively (Olegario et al., 2019). An interesting class of materials for environmental remediation is the modified zeolites, which enhances sorption capacity by introducing complex functional groups (Nasiri-Ardali and Nezamzadeh-Ejhieh, 2020; Shirzadi and Nezamzadeh Ejhieh, 2017), but it is a complicated synthesized process. Besides, the synthesized zeolite has a bigger cation exchange capacity (abbreviated as CEC) than natural zeolite due to no impurities in the ion exchangers and so the uptake capacities of synthesized zeolite NaX for Pb^{2+} and Cu^{2+} are better (UM et al., 2009; Yurekliv, 2019). Despite these signs of progress, to the best of our knowledge, the existing zeolites still suffer from low sorption capacity and removal effectiveness compared to other absorbents. Importantly, many researches about zeolites do not provide the residual concentration of heavy metal after absorption and whether it is up to drinkable level or not is unidentified. Therefore, it is particularly desirable to cultivate an unmodified and reusable zeolite for eradicating heavy metals with great capacity.

Herein, we sought out a zeolite $Na_6Al_6Si_{10}O_{32}\cdot 12H_2O$ (abbreviated as NASO) that a few researches focused on the property of heavy metal removal, and investigated its trapped ability toward heavy metal ions. The synthesized NASO without any modification yielded an absorbent that overcame the limitations mentioned above and manifest effective decontamination of M^{2+} ions (Pb^{2+}, Cd^{2+}, Cu^{2+}, and Zn^{2+}) to drinkable level. To evaluate the absorption performance of NASO, the adsorption isotherms and kinetics were studied to absorption mechanism and acquire maximum capacities that were much better than other modified/unmodified zeolites. The capture abilities of zeolite 4A and 13× to Pb^{2+} ions were for comparison to investigate and conclude the determining factors affecting absorption capacity of zeolite. Because of the energy saving, the regeneration was estimated and proved NASO was a top material for the separation of pollutants.

2. Materials and methods

2.1. Preparation of NASO ($Na_6Al_6Si_{10}O_{32}\cdot 12H_2O$)

All the chemicals used in the experiments were of analytical grade and used without further purification. NASO was synthesized using a facile hydrothermal method. Simply, solution A was prepared by dissolving $Al(NO_3)_3\cdot 9H_2O$ (0.45 g) in 10 mL deionized water. Solution B was got by dissolving $Na_2SiO_3\cdot 9H_2O$ (0.68 g) in 10 mL deionized water. The mixed solution was prepared through the addition of solution B into solution A to form a homogeneous solution with vigorously magnetic stirring for 10 min. Subsequently, NaOH solution (0.23 g NaOH dissolving in 10 mL deionized water) was quickly added, and after 10 min further stirring the resultant solution was sealed in Teflon-lined stainless autoclave (50 mL). The autoclave was heated to

Table 1
Adsorption isotherm data of NASO toward Pb^{2+} ions.

C_0 (mg/L)	C_e (mg/L)	K_d (mL/g)	q_e (mg/g)	Removal (%)
3.9	0.00007	5.57×10^7	3.90	100
10.3	0.00002	5.15×10^8	10.30	100
40.8	0.0003	1.36×10^8	40.80	100
85.5	0.0004	2.14×10^8	85.50	100
131.2	0.0009	1.46×10^8	131.20	100
203.3	0.0077	2.64×10^7	203.29	99.99
400.4	0.2297	1.74×10^6	400.17	99.94
437.9	1.5886	2.75×10^5	436.31	99.64
603.3	38.402	1.47×10^4	564.90	93.63
799.0	147.664	4.41×10^3	651.34	81.52

$m = 0.01$ g, $V = 10$ mL, $V{:}m = 1000$ mL/g, Contact time: 24 h.

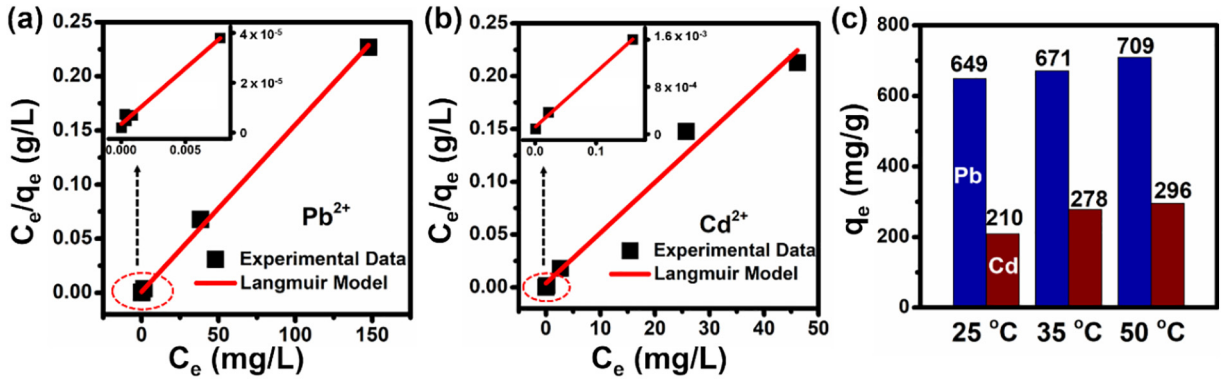

Fig. 3. Sorption isotherms for adsorption of (a) Pb^{2+} and (b) Cd^{2+} by NASO; (c) The maximum capacities for Pb^{2+} and Cd^{2+} at different temperatures.

Table 2
Adsorption isotherm data of NASO toward Pb^{2+} and Cd^{2+} ions.

Temperature	25 °C		35 °C		50 °C	
	Pb^{2+}	Cd^{2+}	Pb^{2+}	Cd^{2+}	Pb^{2+}	Cd^{2+}
Langmuir						
q_{max} (mg/g)	649.4	209.2	671.1	277.8	709.2	295.8
K_L (L/mg)	0.9006	1.2225	0.2321	0.1439	0.2242	0.1556
R^2	0.9980	0.9825	0.9916	0.9414	0.9935	0.9643
Freundlich						
K_F ($mg^{1-n}L^n/g$)	378.9	100.8	198.9	48.8	131.9	53.4
1/n	0.1288	0.2497	0.2599	0.3884	0.3564	0.3858
R^2	0.9315	0.8393	0.8337	0.9369	0.7249	0.8407

160 °C, kept for 24 h, and then samples were cooled to room temperature naturally. After that, the solid material was separated by centrifuging and sequentially washed with deionized water several times to remove the basic solution and then dried at 80 °C for 2 h.

2.2. Batch absorption experiments

The absorption experiments of heavy metal M^{2+} ions (Pb^{2+}, Cd^{2+}, Cu^{2+}, and Zn^{2+}) were performed at ambient temperature using NASO material at the pH values of 3–6 (natural pH values and adjusted with the aid of 1 wt% HNO_3 solution). The individual heavy metal solution under various initial concentrations (5–1000 ppm) was prepared by dissolving $Pb(NO_3)_2$, $Cd(NO_3)_2$, $Cu(NO_3)_2$ and $Zn(NO_3)_2$ in deionized water respectively. The blank experiments without absorbent were also performed which indicated that no addition or loss of heavy metal in the solution. All batch experiments were conducted through dispersing 0.01 g NASO into 10 mL aqueous solutions (V:m = 1000 mL/g) under stirring. The NASO particles were separated by a 0.2 μm nylon filter membrane and the residual solutions were taken to further analysis. The adsorption isotherms at different temperatures were established by adding NASO material to the solution containing individual M^{2+} ions with various initial concentrations (5–1000 ppm) stirred for 24 h. The pH values of low M^{2+} concentrations were 5 adjusted by 1 wt% HNO_3 solution and the pH values of high M^{2+} concentrations were the natural pH about 3–4. Adsorption kinetic experiments for heavy metal M^{2+} ions under different contact time (2–240 min) were conducted.

One measure of sorbent's affinity for the target metal ion is the distribution coefficient (K_d) measurement (Do, 1998). K_d is the ratio of the amount of M^{2+} ions adsorbed by 1 g of the sorbent to that remaining in solution calculated via the Eq. (1):

$$K_d = \frac{V(C_0 - C_e)/C_e}{m} \quad (1)$$

The removal capacity (q_e) is given by the Eq. (2):

$$q_e = \frac{V\,(C_0 - C_e) \times 10^{-3}}{m} \quad (2)$$

The removal % is obtained from the Eq. (3):

$$\text{Removal}\% = \frac{(C_0 - C_e) \times 100}{C_0} \quad (3)$$

where C_0 and C_e are the initial and equilibrium concentrations of heavy metal ions (ppm) after the absorption, respectively; V is the solution volume (L) and m is the adsorbent mass (g).

2.3. Characterization

Powder X-ray diffraction (XRD) measurements were performed on a Bruker D2 phaser diffractometer, operating at 40 kV and 100 mA with Cu Ka radiation (λ = 1.5406 Å). The scanning rate for phase identification was fixed at 5° min^{-1} with a 2θ range from 10° to 60°. The scanning electron microscopy (SEM) images and energy dispersive X-ray spectroscopy (EDS) analyses were attained by a Hitachi S-4800 field-emission electron microscope. The zeta potential of sorbent was measured using a zeta plus (Brookhaven, USA) at various pH from 3 to 6. Teller (BET) method using isotherms collected by an Accelerated Surface Area & Porosimetry system (ASAP2020, Micrometer). The X-ray photoelectron spectroscopy (XPS) was performed by an Axis Ultra Photoelectron Spec-trometer (Kratos Analytical Ltd.) using a monochromatized Al Kα anode (225 W, 15 mA, and 15 kV). The C 1 s peak at 284.8 eV was taken as an internal standard. The FTIR spectrum

Table 3
The physicochemical parameters toward Pb, Cd, Cu and Zn.

Ions	Hydrated ionic radius (Å)	Electronegativity	Hydration enthalpy (ΔH_{H2O} KJ/mol)	Hydrolysis constant $\log K_{MOH}$
Pb^{2+}	4.01	2.33	−1479.9	−7.71
Cd^{2+}	4.26	1.69	−1807	−10.8
Cu^{2+}	4.19	1.90	−2009	−8.00
Zn^{2+}	4.30	1.65	−2046	−8.96

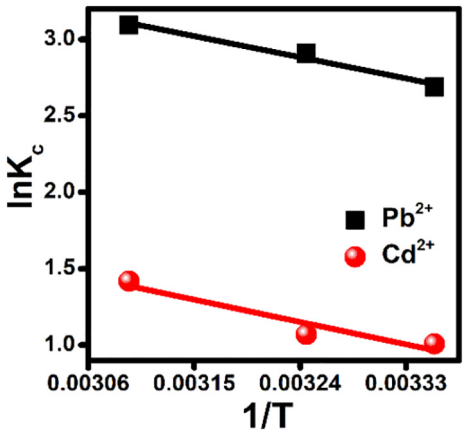

Fig. 4. Plot of lnK_0 vs 1/T for determination of thermodynamic parameters for the adsorption of Pb^{2+} and Cd^{2+}.

were recorded within the range 400–4000 cm^{-1} using an FTIR spectrophotometer (IR-Prestige 21, Shimadzu, Japan) with KBr as the matrix.

The M^{2+} ion concentrations in the range of 1–100 ppm before and after absorption were measured through a Leeman Prodigy 7 spectrometer inductively coupled plasma-atomic emission spectroscopy (ICP-OES). Standards of these ions were prepared by diluting the commercial ~1000 ppm ICP standards, and the calibration was liner with maximum errors of 5%. The equilibrium concentrations of M^{2+} ions in the solutions for extra low concentration (at ppb level) were determined by inductively coupled plasma-mass spectroscopy (ICP-MS) using a PerkinElmer NexION 350× ICP-MS spectrometer.

3. Results and discussion

3.1. Structural analysis of NASO and heavy metal removal

The structure of NASO was, shown in Fig. 1(a), a three-dimensional framework built from corner sharing SiO_4 and AlO_4 tetrahedra linked through oxygen atoms and the dominated channel size was 8.8 Å. The isomorphous replacement of Si^{4+} by Al^{3+} produced negative charges in the lattice balanced via the exchangeable Na ions which were located at the channels. The XRD pattern and SEM image of NASO were depicted in Fig. 1(b) and Fig. 1S(a). It could be observed that all peaks were assigned to the P-type zeolite $Na_6Al_6Si_{10}O_{32}\cdot 12H_2O$ (JCPDS card no. 71-0962) without forming any impurity phase and NASO crystallized in the tetragonal space group I-4 with $a = 10.043$ Å, $c = 10.043$ Å, $V = 1012.96$ $Å^3$. The morphology of NASO was characterized as uniform octahedral with clear crystal edges which confirmed that it was well crystallized in a range of 12–20 μm. The N_2 adsorption and desorption isotherms of NASO were performed at 77 K under 1 bar pressure, shown in Fig. S1(b). The specific surface area calculated by BET method was 10.6 m^2/g and the average pore diameter was 78 Å, which was benefit for ion exchange (Qiu and Zheng, 2009). Because the sizes of most heavy metal cations were below 5 Å. The uptake of M^{2+} ions by NASO from solution in the same concentration (10 ppm) was conducted to explore whether it can be used for the removal of heavy metal ions. The absorption results of individual ions were summarized in Table S1. The adsorption ability toward Pb^{2+} and Cd^{2+} was higher than Cu^{2+}/Zn^{2+}, with the removal rates of near 100%. The SEM and EDS mapping also verified the introduction of M^{2+} ions into NSAO elucidated in Fig. 1(c). Therefore, NASO owned the ability to adsorb heavy metal M^{2+} ions. Finally, the XRD patterns after M^{2+} adsorption were presented in Fig. 1(b) indicating no impurity phase.

Table 4
Thermodynamic parameters for the absorption of Pb^{2+} and Cd^{2+} on NASO.

Sample	Temperature (°C)	ΔG (KJ/mol)	ΔH (KJ/mol)	ΔS (KJ/mol·K)
Pb^{2+}	25	−6.66	12.79	0.065
(C_0 = 600 ppm)	35	−7.22	12.79	0.065
	50	−8.31	12.79	0.065
Cd^{2+}	25	−2.50	13.52	0.053
(C_0 = 300 ppm)	35	−2.74	13.52	0.053
	50	−3.81	13.52	0.053

3.2. Effect of initial pH

Solution pH, one key factor that affected the sorption of heavy metals significantly, determined the metal speciation and surface charge of adsorbent (Jiang et al., 2019). Therefore, the Pb^{2+} removal rates of different initial concentration as a function of pH (3–6) were carried out in batch. At this pH range, precipitation was not the dominant process. From Fig. 2(a), it was apparent that the Pb^{2+} sorption results were favoured at larger pH values. The results were in agreement with the changing of zeta potential of NASO shown in Fig. 2(b), which NASO charges became more negative at higher pH owing to the deprotonation of Si-OH and Al-OH groups ($Si(Al)\text{-}OH + OH^- \rightleftharpoons Si(Al)\text{-}O^- + H_2O$) (Polatoglu and Cakicioglu-Ozkan, 2010). The main Pb^{2+} species were presented as Pb^{2+}, $Pb(OH)^+$ in the pH range of 2–6 at 25 °C (Weng, 2004). Pb^{2+} ions predominate in solution at pH ≤ 5, the competition from H^+ decreased the Pb^{2+} removal via ion exchange and NASO could be dissolved slightly under low pH 2–3 (Anari-Anaraki and Nezamzadeh-Ejhieh, 2015). Meanwhile, more negative charges on the surface of NASO enhanced removal capacity at a bigger pH (Fig. 2(a)). However, for pH = 6, the presence and adsorption of $Pb(OH)^+$ might prevent the diffusion of Pb^{2+} to some sites within the porous structure (Perić et al., 2004). Hence, the pH value was kept at 5.0, which was the same for Cd^{2+}, Cu^{2+}, and Zn^{2+}.

3.3. Sorption isotherm toward M^{2+} and removal capacity

Based on the above results, NASO disclosed acceptable sorption for M^{2+}. The batch sorption experiments at ambient temperature within a wide range of M^{2+} concentrations were conducted. The initial and residual concentrations of M^{2+} in the aqueous solution could be acquired through ICP measurements. As shown in Tables 1 and S2, the M^{2+} ions captured by NASO increased significantly with the increasing of initial concentrations. On a broad range of initial concentration (4–400 ppm), the Pb^{2+} removal rates reached >99.9% and K_d values ranged from 1.74×10^6 to 5.15×10^8 mL/g. K_d represents the performance metrics of metal ion removal for any sorbent, and K_d values of 1.0×10^5 mL/g are considered excellent (Li et al., 2014; Shin et al., 2007). The removal rates of Cd^{2+} were > 99.85% with the initial concentration of 10–100 ppm and the corresponding K_d values were about 10^5–10^7 mL/g. For Cu^{2+}, the removal rates were > 99.83% ($K_d \approx 10^5$–10^6 mL/g) in a small range of 10–60 ppm. For Zn^{2+}, the removal rates were relatively lower at >99.47% ($K_d \approx 10^5$ mL/g) with the initial concentration of 5–50 ppm.

The uptake capacity of NASO, another significant aspect of sorbent's performance metric, was calculated by Langmuir and Freundlich

Table 5
Kinetics data of Pb^{2+} adsorption using NASO.

C_0 (mg/L)	Time (min)	C_e (mg/L)	K_d (mL/g)	q_t (mg/g)	t/qt (min·g/mg)
7.5	2	0.0006	1.25×10^7	7.499	99.99
	5	0.0009	8.33×10^6	7.499	99.98
	10	0.0005	1.50×10^7	7.500	99.99
	30	0.0006	1.25×10^7	7.499	99.99

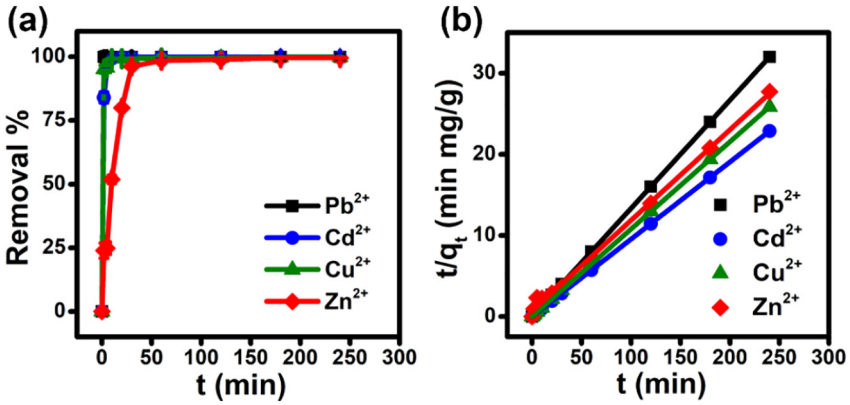

Fig. 5. Adsorption kinetics curves for Pb^{2+}, Cd^{2+}, Cu^{2+}, and Zn^{2+}: (a) removal % as a function of contact time; (b) Pseudo-second-order kinetic plots for ion adsorption.

isotherms which were expressed as following (4–5) (Nezamzadeh-Ejhieh and Kabiri-Samani, 2013):

$$\frac{C_e}{q_e} = \frac{1}{q_{max}K_L} + \frac{C_e}{q_{max}} \tag{4}$$

$$\ln q_e = \ln K_F + \frac{1}{n}\ln C_e \tag{5}$$

where q_e (mg/g) is the amount of the heavy metal absorbed at equilibrium concentration, C_e (mg/L) is the equilibrium concentration, q_{max} is the maximum theoretical sorption capacity of the adsorbent, n is the heterogeneity factor related to the adsorption intensity of absorbent, K_L (L/mg) and K_F (mg/g (mg/L)$^{-1/n}$) represent the Langmuir and Freundlich constants, respectively.

The adsorption isotherms of M^{2+} on NASO were interpreted in Figs. 3 and S2, and all the sorption parameters were concluded by the two isotherm equations presented in Table 2. The maximum Pb^{2+} removal capacity reached ~649 mg/g and the correlation coefficient yielded to 0.998. The Langmuir isotherm model better described the equilibrium data, which implied that the adsorption of M^{2+} on NASO was typical monomolecular-layer adsorption with homogeneous binding sites. We also picked up the adsorption capacity of NASO material for Cd^{2+}, Cu^{2+} and Zn^{2+} and found thatNASO had a maximum adsorption capacity ~210 mg/g for Cd^{2+}. The maximum adsorption capacities for Cu^{2+} and Zn^{2+} were relatively lower at 90 mg/g and 88 mg/g respectively. The uptake capacities of Pb^{2+} and Cd^{2+} could be enhanced by increasing the operation temperature viewed in Fig. 3(c) which was attributed to the bigger kinetic energy of cations at elevated temperature (Li et al., 2019). This was comparable for the other adsorbents as given in Table S3.

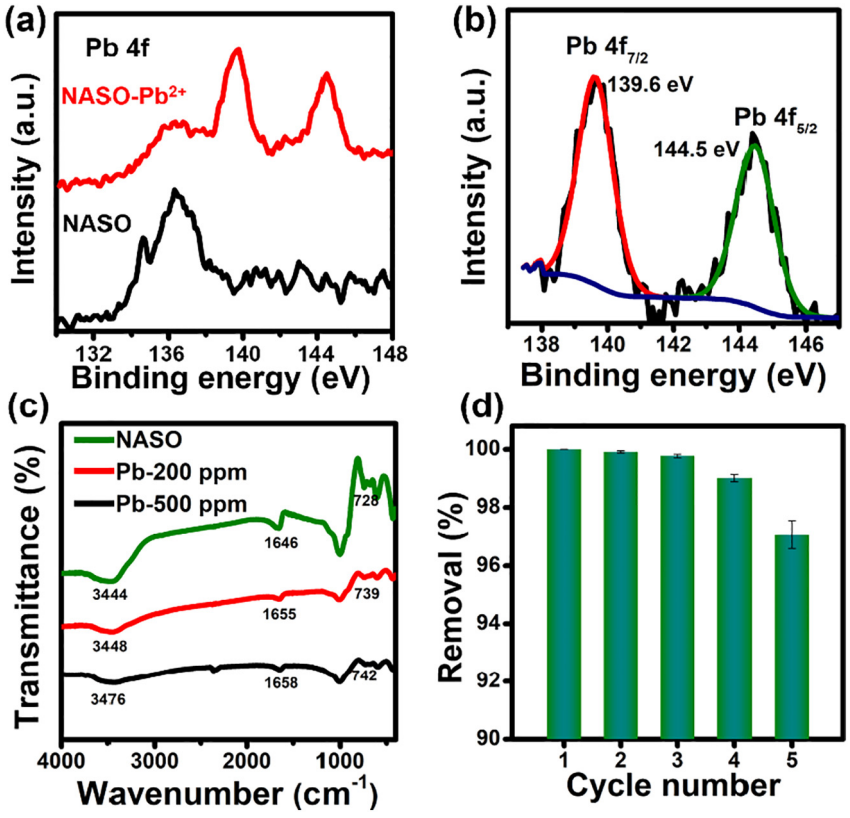

Fig. 6. (a) XPS spectra of Pb 4f before and after Pb^{2+} absorption; (b) deconvoluted Pb 4f spectra of Pb^{2+} adsorbed sample; (c) FTIR spectra of NASO before and after adsorption of Pb^{2+}; (d) Recycle performance of NASO toward Pb^{2+}.

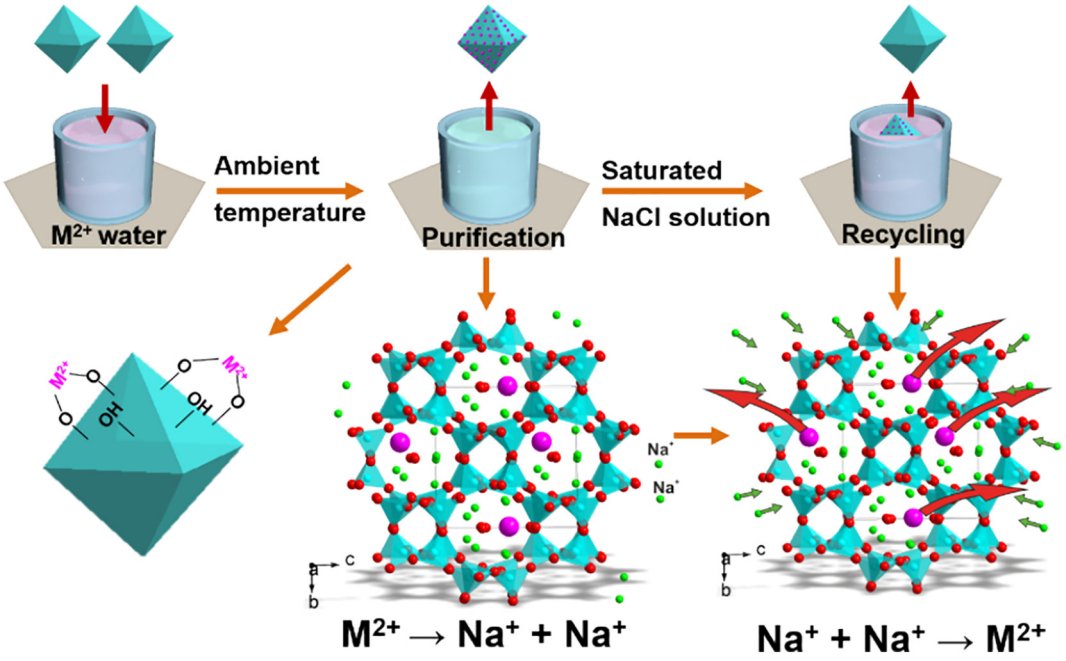

Fig. 7. Schematic diagram of the adsorption and desorption of M^{2+} on NASO.

The analysis of uptake capacities of four metals at the same condition disclosed that adsorbent affinity followed the order $Pb^{2+} > Cd^{2+} > Cu^{2+} > Zn^{2+}$, which was assigned to the physicochemical properties of heavy metals including electronegativity, hydration radius, first hydrolysis constant and hydration enthalpy (Yurekliv, 2019). The difference in hydration radius of metal ions was one factor in the ion exchange process. The lower hydration radius of Pb^{2+} ($Pb^{2+} < Cu^{2+} < Cd^{2+} < Zn^{2+}$) (Nightingale Jr, 1959), presented in Table 3, could pass readily through the channels (8.8 Å) resulting in the biggest capacity. The larger hydration enthalpy (ΔH_{H2O}) of metals ($Pb^{2+} > Cd^{2+} > Cu^{2+} > Zn^{2+}$) would boost the adsorption capacity (Hawari et al., 2014; Rudolph and Pye, 1999; Uudsemaa and Tamm, 2004). This was exactly what was observed in this study. The first hydrolysis constants could also be evidence for sorption ability and the higher $\log K_{MOH}$ value exhibited greater sorption capacity (Pagnanelli et al., 2003). The $\log K_{MOH}$ values for four metals were $Pb^{2+} > Cu^{2+} > Zn^{2+} > Cd^{2+}$ listed in Table 3. Likewise, the Pauling electronegativity values followed as $Pb^{2+} > Cu^{2+} > Cd^{2+} > Zn^{2+}$ reflecting Pb^{2+} possessed the greatest ionic potential (Yurekliv, 2019). Hence, Pb^{2+} had the strongest attraction to NASO and the sorption ability was $Pb^{2+} > Cu^{2+} > Zn^{2+}$, which was consistent with the experimental results of sorption capacity. The abnormal Cd^{2+} sorption capacity might be dominated by the hydration enthalpy that was greater than Cu^{2+} and Zn^{2+}.

3.4. Thermodynamic parameters

The absorption capacities of Pb^{2+} and Cd^{2+} could be enhanced by increasing reaction temperature. To investigate the influence of temperature on the adsorption, the thermodynamic parameters including free energy change (ΔG), enthalpy change (ΔH), and entropy change (ΔS) were calculated by following equations:

$$\Delta G = -RT \ln K_c \tag{6}$$

where K_c is the thermodynamic equilibrium constant without units, T represents the absolute temperature (K), and R is the gas constant 8.314 $J \cdot mol^{-1} \cdot K^{-1}$. The ΔH and ΔS can be acquired according to Eqs. (7)–(9):

$$\Delta G = \Delta H - T\Delta S \tag{7}$$

$$\ln K_c = \frac{\Delta S}{R} - \frac{\Delta H}{RT} \tag{8}$$

$$K_c = \frac{C_{ad}}{C_e} \tag{9}$$

The thermodynamic equilibrium constant K_c is expressed based on the distribution constant (Chen et al., 2011; Liu, 2009). C_e and C_{ad} are the concentration of heavy metal in solution and adsorbed on NASO at equilibrium. The values of ΔS and ΔH were calculated from the intercept and slope of the plots of $\ln K_c$ versus $1/T$ as shown in Fig. 4. The thermodynamic parameters were listed in Table 4. The positive enthalpy change confirmed that the absorption process was endothermic, which led to improve adsorption capacities under higher temperature. The negative values of free energy change decreased with increasing

Table 6
The adsorption capacities of various zeolites for heavy metal ions.

Absorbent	Metal	q_{max} (mg/g)	Ref
Cancrinite-type zeolite	Pb^{2+}	524	(Qiu and Zheng, 2009)
	Cu^{2+}	132	
	Zn^{2+}	75	
LTA zeolite	Pb^{2+}	510	(Hong et al., 2019)
Zeolite A	Pb^{2+}	228	(Meng et al., 2017)
Faujasite zeolite	Cu^{2+}	94	(Chen et al., 2020)
NaX zeolite	Pb^{2+}	255	(Yurekliv, 2019)
	Cu^{2+}	140	
Clinoptilolite	Pb^{2+}	182	(Li et al., 2019)
	Cd^{2+}	45	
	Cu^{2+}	34	
	Zn^{2+}	31	
Modified clinoptilolite	Cd^{2+}	139	(Sadat Shafiof and Nezamzadeh-Ejhieh, 2020)
PAN-NaY-zeolite	Pb^{2+}	74	(Elwakeel et al., 2018)
	Cd^{2+}	42	
	Cu^{2+}	44	
Synthetic NASO	Pb^{2+}	649	This work
	Cd^{2+}	210	
	Cu^{2+}	90	
	Zn^{2+}	88	

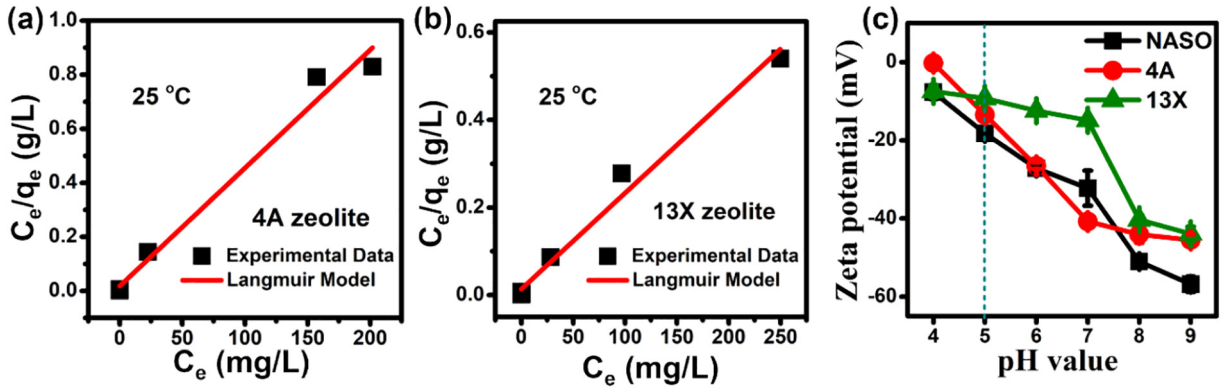

Fig. 8. Sorption isotherms for adsorption of Pb^{2+} by (a) 4A and (b) 13X; (c) zeta potential measurement plots of zeolite 4A, 13X and NASO at different pH values.

temperature indicated that the adsorption of Pb^{2+} and Cd^{2+} was feasible and spontaneous. The positive values of entropy change reflected the increased randomness at the solid-solution interface during adsorption (Radi et al., 2019). The high temperature was more favourable to the absorption of M^{2+} on NASO.

3.5. Adsorption kinetics study

The efficiency of NASO for heavy metal removal from aqueous solutions had been examined by studying the adsorption kinetics. The influence of contact time of M^{2+} ions with NASO was explored to determine adsorption rates and equilibrium times. As depicted in Tables 5, S4 and Fig. 5(a), the adsorption rate for 7.5 ppm Pb^{2+} was especially fast and the residual concentration could be limited to 0.6 ppb within 2 min, the removal rate reached 99.99% and K_d value was 10^7 mL/g. Nevertheless, the 170 ppm Pb^{2+} could be eliminated to 4.313 ppm within 5 min and the adsorption equilibrium was acquired within 12 h. The ion exchange of zeolite occurred over two distinct stages: fast adsorption on the surface and diffusion in the interior of zeolite (Hui et al., 2005). Consequently, the 7.5 ppm Pb^{2+} was adsorbed quickly on the surface of NASO. With the increasing of Pb^{2+} concentration, the absorption rate was fast during the early stage owing to many active sites. Then it took more time to achieve adsorption equilibrium which might be due to the following reasons: (1) the lower Pb^{2+} concentration at the final stage reduced the driving force for ion exchange between NASO and Pb^{2+}, (2) the diffusion of Pb^{2+} in the interior took longer time. The capture rate for Cd^{2+} was a little lower than Pb^{2+} under the same experimental conditions, the residual concentration and removal rate was up to 6 ppb ($K_d = 10^5$ mL/g) and 99.5% within 30 min respectively. The removal rate of Cu^{2+} achieved 99.5% within 60 min, but the subsequent capture became slower and needed more time to reach equilibrium. For Zn^{2+} ions, the removal rate was slow but still 98.5% in 120 min.

Generally, the adsorption rates were determined via Pseudo-first-order and Pseudo-second-order models to reveal adsorption behaviors based on the experimental data. The two kinetic rate equations were as follows:

Pseudo-first-order (10):

$$\ln(q_e - q_t) = \ln q_e - k_1 t \tag{10}$$

Pseudo-second-order (11):

$$\frac{t}{q_t} = \frac{1}{k_2 q_e^2} + \frac{t}{q_e} \tag{11}$$

where q_e and q_t (mg/g) are the amount of heavy metal absorbed at equilibrium concentration and at time t, while k_1 (min^{-1}) and k_2 (g/mg min^{-1}) are the Pseudo-first-order and Pseudo-second-order adsorption rate constants respectively. From Fig. 5(b), it was observed that the plots of t/q_t vs t of the kinetics data toward four ions Pb^{2+}, Cd^{2+}, Cu^{2+}, and Zn^{2+} exhibited perfect linear relations with high correlation coefficients R^2 closed to 1. The calculated removal capacities (q_e, cal) of Pb^{2+}, Cd^{2+}, and Cu^{2+} received from the Pseudo-second order model were closer to the corresponding experimental values (q_e, exp) as summarized in Table S5. The results indicated all data could be well described via the Pseudo-second-order kinetic model, signifying that the M^{2+} removal was chemical adsorption.

3.6. Absorption mechanism

As stated, the amount of Na^+ ions in 1 g $Na_6Al_6Si_{10}O_{32}\cdot 12H_2O$ was 4.59 mmol. To keep the charge balance, the ion exchange equation was $2Na^+ \rightarrow Pb^{2+}$, the theoretical maximum exchange amount of Pb^{2+} ions would be 2.29 mmol. However, the maximum removal capacity of Pb^{2+} was 3.14 mmol (649 mg/g). According to ICP analysis, the amount of Na in 0.01 g NASO was 0.0441 mmol and the residual amount of Na in NASO absorbed by 200 ppm Pb^{2+} was 0.0202 mmol. Accordingly, we supposed that there were two components of Pb^{2+} adsorption: (1) Pb^{2+} ions were exchanged by Na^+ ions; (2) Pb^{2+} reacted with the OH groups of the NASO. To better understand the adsorption mechanism, the infrared spectrum (400–4000 cm^{-1}) and XPS analysis of NASO samples before and after Pb^{2+} adsorption were executed presented in Fig. 6. As illustrated in Fig. 6(a), (b), two peaks appeared at 139.6 eV and 144.3 eV assigned to Pb $4f_{7/2}$ and Pb $4f_{5/2}$ respectively, which advocated that Pb^{2+} was successfully adsorbed on NASO. Additionally, the intensity of peak at 1071 eV (Na 1 s) decreased after Pb^{2+} adsorption, indicating that Na^+ ions were exchanged by Pb^{2+} (Fig. S3). In the FTIR spectra (Fig. 6(c)), the bands at 446 cm^{-1}, 929 cm^{-1} and 742 cm^{-1} were corresponding to the bending vibration of $Si(Al)O_4$ tetrahedra, symmetric stretching vibrations of Si-O-Si or Si-O-Al bridges and Al-OH bending vibration, respectively (Yurekliv,

Table 7
The adsorption capacities of various zeolites for Pb^{2+} ions.

Zeolite	Composition	Pore size (Å)	Theoretical CEC (mmol/g)	Zeta potential pH = 5	Pb^{2+} q_{max} (mmol/g)
4A	$Na_{12}Al_{12}Si_{12}O_{48}\cdot 27H_2O$	4.2	5.4 → 2.7 Pb^{2+}	−13.48	1.37
13X	$Na_2Al_2Si_{2.46}O_{8.9}\cdot 6H_2O$	8	4.77 → 2.39	−9.28	2.61
NASO	$Na_6Al_6Si_{10}O_{32}\cdot 12H_2O$	8.8	4.59 → 2.29	−18.2	3.14

2019). The strong vibration at 1006 cm^{-1} was correlated with Si(Al)-O asymmetric stretching (Nibou et al., 2011). The characteristic peaks at 1658 cm^{-1} and 3476 cm^{-1} were associated with the bending vibration of -OH (Tabit et al., 2019). After Pb^{2+} absorption, the intensities of peaks at 1658 cm^{-1} and 3476 cm^{-1} reduced originated from the Pb—O vibrations. Furthermore, the peaks at 742, 1658 and 3476 cm^{-1} shifted to 728, 1646 and 3444 cm^{-1} respectively, confirming the involvement of hydroxyl groups in the Pb^{2+} removal process (Chen et al., 2020). The above results proved the proposed absorption mechanism and the schematic diagram of the adsorption mechanism was given in Fig. 7.

3.7. Comparison of the heavy metal removal efficiency of NASO with other zeolites

To the best of our knowledge, the Pb^{2+} uptake capacity of NASO was the top among zeolites reported for heavy metal adsorption (Table 6). Based on the analysis of absorption mechanism, we proposed the heavy metal uptake capacity of zeolites depended on: (1) cation exchange capacity (CEC), (2) pore size on the zeolite framework, (3) the OH groups of zeolites and (4) phase purity. So, we investigated the cation capacity, zeta potential and Pb^{2+} uptake capacity of commercial zeolite 4A and 13X for comparison displayed in Fig. 8 and Table 7.

Comparing with the pore size of three zeolites, it was apparent that all the unhydrated and hydrated M^{2+} ions could diffuse to the channels of zeolites, but the radius of hydrated ions was approximately the same as the channel size of zeolite 4A and they might exchange with difficulty. Meanwhile, the lower zeta potential of NASO led to a greater uptake capacity of Pb^{2+} compared with zeolite 13X. Furthermore, the zeolite crystallinity and no impurity phase played important role in determining the heavy metal adsorption capacity. The NASO with much impurity phase prepared by using coal bottom ash revealed a low capacity of Pb^{2+} and Cd^{2+} (15.4 and 12.7 mg/g) (UM et al., 2009). Because some present cations for ion exchange were components of impurities or they were located at inaccessible sites of the material structure, which were not suitable for ion exchange. On that account, the uptake capacities of heavy metal on the same type of zeolites were significant variation.

3.8. Competitive and effect of co-existing ions experiments

Moreover, complex competitive effects of different heavy metals in the real wastewater should be considered and the competitive experiments were conducted through mixing four ions with the same concentration. The results, listed in Table S6, made known that the selectivity order was $Pb^{2+} > Cu^{2+} > Cd^{2+} > Zn^{2+}$ which was the same as the order of Pauling electronegativity. This indicated that NASO was very selective for ions with high electronegativity. However, the selectivity of Cu^{2+}, Cd^{2+} and Zn^{2+} was relatively low at high initial concentration. Meanwhile, we also examined the influence of co-existing ions (100 ppm Na and 100 ppm Ca) on the absorption of single ion (10 ppm) and mixed ions (10 ppm). For single Cd^{2+}, Cu^{2+} or Zn^{2+} ions, the presence of Na and Ca caused a reduction in the adsorption capacity. Nevertheless, it had no effect on the adsorption of Pb^{2+} whatever it was single ions or mixed ions as shown in Table S7.

3.9. Reusable capacity of NASO

The reusability of absorption materials was an essential factor for practical application. Therefore, the desorption experiments were conducted to assess the regeneration feature of exhausted NASO via using a saturated NaCl solution as the eluting agent. The regeneration mechanism was ion exchange ($Pb^{2+} \rightarrow 2Na^{+}$) depicted in Fig. 7. For the absorption of 200 ppm Pb^{2+}, the Pb^{2+} removal rate of fresh adsorbents attained to 99.95%, and then a little loss of adsorption capacity (removal % = 97%) was observed after continuous five cycles in Fig. 6(d), signifying that NASO was repeatable and could be candidate for practical pollutant removal.

4. Conclusion

In conclusion, we found an unmodified and reusable zeolite $Na_6Al_6Si_{10}O_{32}\cdot 12H_2O$ for eradicating heavy metal accompanied by great capacity. The pure NASO with uniform octahedral shape was firstly prepared by regulating the ratio of Al/Si/NaOH/H_2O. The maximum capacities of Pb^{2+}, Cd^{2+}, Cu^{2+}, and Zn^{2+} were 649, 210, 90 and 88 mg/g on NASO which was better than other zeolites as we have known. The NASO could diminish Pb^{2+}concentration (4–130 ppm) down to <1 ppb and the distribution coefficients (K_d) reached ~10^8 mL/g. Fast adsorption was observed that Pb^{2+} concentration (7.5 ppm) could be reduced to 0.6 ppb in 2 min. It also explained the relationship between adsorbent affinity and physicochemical properties of heavy metals. The removal mechanism was accredited to the ion exchange and hydroxyl groups on the surface of NASO. Based on the comparison of other zeolites, we proposed and verified the insights impacting the absorption capacity of zeolites. The presence of coexisting ions (Na and Ca) had no influence on the removal efficiency of Pb^{2+} and the removal rate of Pb^{2+} still kept 97%, after five regeneration recycles. The NASO was thus a promising absorbent for practical pollutant treatment and industrialization.

CRediT authorship contribution statement

Mingyue Chen: Conceptualization, Methodology, Data curation, Validation, Formal analysis, Software, Investigation, Writing - original draft, Writing - review & editing.**Shuying Nong:**Validation, Formal analysis, Methodology, Writing - review & editing.**Yantao Zhao:**Software, Resources, Methodology.**Muhammad Sohail Riaz:**Writing - review & editing.**Yi Xiao:**Software, Resources.**Maxim S. Molokeev:**Software, Formal analysis.**Fuqiang Huang:**Formal analysis, Writing - review & editing, Supervision, Funding acquisition.

Declaration of competing interest

The authors declare that they have no competing financial interests or personal relationships that could have appeared to influence the work reported in the paper.

Acknowledgements

This work was supported by the National Key Research and Development Program of China (Grant No. 2016YFB0901600); National Science Foundation of China (Grant No. 21871008); Science and Technology Commission of Shanghai Municipality (Grant No. 14520722000) and China Postdoctoral Science Foundation [Grant No. 8206300161]. Thank Shuying Nong for her experimental assistance.

Appendix A. Supplementary data

Supplementary data to this article can be found online at https://doi.org/10.1016/j.scitotenv.2020.138535.

References

Anari-Anaraki, M., Nezamzadeh-Ejhieh, A., 2015. Modification of an Iranian clinoptilolite nano-particles by hexadecyltrimethyl ammonium cationic surfactant and dithizone for removal of Pb(II) from aqueous solution. J Colloid Interf Sci 440, 272–281.

Bolisetty, S., Mezzenga, R., 2016. Amyloid-carbon hybrid membranes for universal water purification. Nat. Nanotechnol. 11, 365.

Chen, S.H., Yue, Q.Y., Gao, B.Y., Li, Q., Xu, X., 2011. Removal of Cr (VI) from aqueous solution using modified corn stalks: characteristic, equilibrium, kinetic and thermodynamic study. Chem. Eng. J. 168, 909–917.

Chen, Y., Armutlulu, A., Sun, W.L., Jiang, W.J., Jiang, X., Lai, B., et al., 2020. Ultrafast removal of Cu(II) by a novel hierarchically structured faujasite-type zeolite fabricated from lithium silica fume. Sci. Total Environ. 136724.
Do, D.D., 1998. Adsorption Analysis: Equilibria and Kinetics. Imperial College Press, London.
Elwakeel, K., El-Bindary, A., Kouta, E., Guibal, E., 2018. Functionalization of polyacrylonitrile/Na-Y-zeolite composite with amidoxime groups for the sorption of Cu(II), Cd(II) and Pb(II) metal ions. Chem. Eng. J. 332, 727–736.
Gossuin, Y., Hantson, A.-L., Vuong, Q.L., 2020. Low resolution benchtop nuclear magnetic resonance for the follow-up of the removal of Cu^{2+} and Cr^{3+} from water by amberlite IR120 ion exchange resin. J Water Process Eng 33, 101024.
Hawari, A., Khraisheh, M., Al-Ghouti, M.A., 2014. Characteristics of olive mill solid residue and its application in remediation of Pb^{2+}, Cu^{2+} and Ni^{2+} from aqueous solution: mechanistic study. Chem. Eng. J. 251, 329–336.
Hong, M., Yu, L.Y., Wang, Y.D., Zhang, J., Chen, Z.W., Dong, L., et al., 2019. Heavy metal adsorption with zeolites: the role of hierarchical pore architecture. Chem. Eng. J. 359, 363–372.
Hui, K., Chao, C.Y.H., Kot, S., 2005. Removal of mixed heavy metal ions in wastewater by zeolite 4A and residual products from recycled coal fly ash. J. Hazard. Mater. 127, 89–101.
Jawed, A., Saxena, V., Pandey, L.M., 2020. Engineered nanomaterials and their surface functionalization for the removal of heavy metals: a review. J Water Process Eng 33, 101009.
Jiang, D.M., Yang, Y.H., Huang, C.T., Huang, M.Y., Chen, J.J., Rao, T.D., et al., 2019. Removal of the heavy metal ion nickel (II) via an adsorption method using flower globular magnesium hydroxide. J. Hazard. Mater. 373, 131–140.
Li, B.Y., Zhang, Y.M., Ma, D.X., Shi, Z., Ma, S.Q., 2014. Mercury nano-trap for effective and efficient removal of mercury (II) from aqueous solution. Nat. Commun. 5, 5537.
Li, Y.R., Bai, P., Yan, Y., Yan, W.F., Shi, W., Xu, R.R., 2019. Removal of Zn^{2+}, Pb^{2+}, Cd^{2+}, and Cu^{2+} from aqueous solution by synthetic clinoptilolite. Micropor Mesopor Mat 273, 203–211.
Liu, Y., 2009. Is the free energy change of adsorption correctly calculated? J. Chem. Eng. Data 54, 1981–1985.
Ma, L.J., Wang, Q., Islam, S.M., Liu, Y.C., Ma, S.L., Kanatzidis, M.G., 2016. Highly selective and efficient removal of heavy metals by layered double hydroxide intercalated with the MoS_4^{2-} ion. J. Am. Chem. Soc. 138, 2858–2866.
Manos, M.J., Kanatzidis, M.G., 2009. Sequestration of heavy metals from water with layered metal sulfides. Chem-Eur. J. 15, 4779–4784.
Meng, Q.P., Chen, H., Lin, J.Z., Lin, Z., Sun, J.L., 2017. Zeolite A synthesized from alkaline assisted pre-activated halloysite for efficient heavy metal removal in polluted river water and industrial wastewater. J. Environ. Sci. 56, 254–262.
Mukhopadhyay, R., Bhaduri, D., Sarkar, B., Rusmin, R., Hou, D.Y., Khanam, R., et al., 2020. Clay–polymer nanocomposites: progress and challenges for use in sustainable water treatment. J. Hazard. Mater. 383, 121125.
Nasiri-Ardali, M., Nezamzadeh-Ejhieh, A., 2020. A comprehensive study on the kinetics and thermodynamic aspects of batch and column removal of Pb(II) by the clinoptilolite-glycine adsorbent. Mater. Chem. Phys. 240, 122142.
Nezamzadeh-Ejhieh, A., Kabiri-Samani, M., 2013. Effective removal of Ni (II) from aqueous solutions by modification of nano particles of clinoptilolite with dimethylglyoxime. J. Hazard. Mater. 260, 339–349.
Nibou, D., Khemaissia, S., Amokrane, S., Barkat, M., Chegrouche, S., Mellah, A., 2011. Removal of UO_2^{2+} onto synthetic NaA zeolite. Characterization, equilibrium and kinetic studies. Chem. Eng. J. 172, 296–305.
Nightingale Jr., E., 1959. Phenomenological theory of ion solvation. Effective radii of hydrated ions. J. Phys. Chem. C 63, 1381–1387.
Olegario, E., Pelicano, C.M., Felizco, J.C., Mendoza, H., 2019. Thermal stability and heavy metal (As^{5+}, Cu^{2+}, Ni^{2+}, Pb^{2+} and Zn^{2+}) ions uptake of the natural zeolites from the Philippines. Mater Res Express 6, 085204.
Pagnanelli, F., Esposito, A., Toro, L., Veglio, F., 2003. Metal speciation and pH effect on Pb, Cu, Zn and Cd biosorption onto Sphaerotilus natans: Langmuir-type empirical model. Water Res. 37, 627–633.
Perić, J., Trgo, M., Medvidović, N.V., 2004. Removal of zinc, copper and lead by natural zeolite-a comparison of adsorption isotherms. Chem. Eng. J. 38, 1893–1899.
Polatoglu, I., Cakicioglu-Ozkan, F., 2010. Aqueous interactions of zeolitic material in acidic and basic solutions. Micropor Mesopor Mat 132, 219–225.
Qiu, W., Zheng, Y., 2009. Removal of lead, copper, nickel, cobalt, and zinc from water by a cancrinite-type zeolite synthesized from fly ash. Chem. Eng. J. 145, 483–488.
Radi, S., El Abiad, C., Moura, N.M., Faustino, M.A., Neves, M.G.P., 2019. New hybrid adsorbent based on porphyrin functionalized silica for heavy metals removal: synthesis, characterization, isotherms, kinetics and thermodynamics studies. J. Hazard. Mater. 370, 80–90.
Rathore, E., Pal, P., Biswas, K., 2017. Layered metal chalcophosphate (K-MPS-1) for efficient, selective, and ppb level sequestration of Pb from water. J. Phys. Chem. C 121, 7959–7966.
Rudolph, W.W., Pye, C.C., 1999. Zinc(II) hydration in aqueous solution. A Raman spectroscopic investigation and an ab-initio molecular orbital study. Phys. Chem. Chem. Phys. 1, 4583–4593.
Sadat Shafiof, M., Nezamzadeh-Ejhieh, A., 2020. A comprehensive study on the removal of Cd(II) from aqueous solution on a novel pentetic acid-clinoptilolite nanoparticles adsorbent: experimental design, kinetic and thermodynamic aspects. Solid State Sci. 99, 106071.
Sarma, D., Islam, S.M., Subrahmanyam, K., Kanatzidis, M.G., 2016. Efficient and selective heavy metal sequestration from water by using layered sulfide $K_{2x}Sn_{4-x}S_{8-x}$ ($x = 0.65$-1; KTS-3). J. Mater. Chem. A 4, 16597–16605.
Sdiri, A., Higashi, T., Hatta, T., Jamoussi, F., Tase, N., 2011. Evaluating the adsorptive capacity of montmorillonitic and calcareous clays on the removal of several heavy metals in aqueous systems. Chem. Eng. J. 172, 37–46.
Shin, Y., Fryxell, G.E., Um, W., Parker, K., Mattigod, S.V., Skaggs, R., 2007. Sulfur-functionalized mesoporous carbon. Adv. Funct. Mater. 17, 2897–2901.
Shirzadi, H., Nezamzadeh Ejhieh, A., 2017. An efficient modified zeolite for simultaneous removal of Pb(II) and Hg(II) from aqueous solution. J. Mol. Liq. 230, 221–229.
Tabit, K., Waqif, M., Saâdi, L., 2019. Application of the Taguchi method to investigate the effects of experimental parameters in hydrothermal synthesis of Na-P1 zeolite from coal fly ash. Res. Chem. Intermed. 1–17.
Uddin, M.K., 2017. A review on the adsorption of heavy metals by clay minerals, with special focus on the past decade. Chem. Eng. J. 308, 438–462.
UM, N.I., HAN, G.C., You, K.S., Ahn, J.W., 2009. Immobilization of Pb, Cd and Cr by synthetic NaP1 zeolites from coal bottom ash treated by density separation. Resources Processing 56, 130–137.
Uudsemaa, M., Tamm, T., 2004. Calculation of hydration enthalpies of aqueous transition metal cations using two coordination shells and central ion substitution. Chem. Phys. Lett. 400, 54–58.
Wang, R.Q., Chen, H.J., Xiao, Y., Hadar, I., Bu, K.J., Zhang, X., et al., 2019a. $K_x[Bi_{4-x}Mn_xS_6]$, design of a highly selective ion exchange material and direct gap 2D semiconductor. J. Am. Chem. Soc. 141, 16903–16914.
Wang, Y.C., Gu, Y., Xie, D.H., Qin, W.X., Zhang, H.M., Wang, G.Z., et al., 2019b. A hierarchical hybrid monolith: MoS_4^{2-}-intercalated NiFe layered double hydroxide nanosheet arrays assembled on carbon foam for highly efficient heavy metal removal. J. Mater. Chem. A 7, 12869–12881.
Weng, C.-H., 2004. Modeling Pb(II) adsorption onto sandy loam soil. J Colloid Inter Sci 272, 262–270.
Wu, Y., Qiu, X.D., Cao, S.Y., Chen, J.J., Shi, X.W., Du, Y.M., et al., 2019. Adsorption of natural composite sandwich-like nanofibrous mats for heavy metals in aquatic environment. J Colloid Interf Sci 539, 533–544.
Yang, X.D., Wan, Y.S., Zheng, Y.L., He, F., Yu, Z.B., Huang, J., et al., 2019. Surface functional groups of carbon-based adsorbents and their roles in the removal of heavy metals from aqueous solutions: a critical review. Chem. Eng. J. 608–621.
Yurekliv, Y., 2019. Determination of adsorption characteristics of synthetic NaX nanoparticles. J. Hazard. Mater. 120743.
Zhao, G.X., Li, J.X., Xm, Ren, Chen, C.L., Wang, X.K., 2011. Few-layered graphene oxide nanosheets as superior sorbents for heavy metal ion pollution management. Environ Sci Technol 45, 10454–10462.